Earth and Planetary Science Letters 551 (2020) 116544

Contents lists available at ScienceDirect

Earth and Planetary Science Letters

www.elsevier.com/locate/epsl

Chondritic mercury isotopic composition of Earth and evidence for evaporative equilibrium degassing during the formation of eucrites

Frédéric Moynier [a,b,*], Jiubin Chen [c,a], Ke Zhang [c], Hongming Cai [c], Zaicong Wang [a], Matthew G. Jackson [d], James M.D. Day [e]

[a] State Key Laboratory of Geological Processes and Mineral Resources, School of Earth Sciences, China University of Geosciences, Wuhan 430074, China
[b] Institut de Physique du Globe de Paris, Université de Paris, CNRS, 1 rue Jussieu, Paris 75005, France
[c] Institute of Surface-Earth System Science, Tianjin University, China
[d] Department of Earth Science, University of California, Santa Barbara, CA 93106, USA
[e] Scripps Institution of Oceanography, University of California San Diego, La Jolla, CA 92093-0244, USA

ARTICLE INFO

Article history:
Received 20 March 2020
Received in revised form 19 August 2020
Accepted 21 August 2020
Available online 9 September 2020
Editor: R. Dasgupta

Keywords:
Hg isotopes
MIF
volatilization
late accretion
volatile elements

ABSTRACT

Variations in the abundances of moderately volatile elements (MVE) are one of the most fundamental geochemical differences between the terrestrial planets. Whether these variations are the consequence of nebular processes, planetary volatilization, differentiation or late accretion is still unresolved. The element mercury is the most volatile of the MVE and is a strongly chalcophile element. It is one of the few elements that exhibit large mass-dependent (MDF) and mass-independent (MIF) isotopic fractionations for both odd (odd-MIF, Δ^{199}Hg and Δ^{201}Hg) and even (even-MIF, Δ^{200}Hg) Hg isotopes in nature, which is traditionally used to trace Hg biogeochemical cycling in surface environments. However, the Hg isotopic composition of Earth and meteorites is not well constrained. Here, we present Hg isotopic data for terrestrial basaltic, trachytic and granitic igneous samples. These rocks are isotopically lighter (δ^{202}Hg $= -3.3 \pm 0.9$‰; 1 standard deviation) than sedimentary rocks that have previously been considered to represent the terrestrial Hg isotope composition (δ^{202}Hg $= -0.7 \pm 0.5$‰; 1 standard deviation). We show degassing during magma emplacement induces MIF that are consistent with kinetic fractionation in these samples. Also presented is a more complete dataset for chondritic (carbonaceous, ordinary and enstatite) meteorites, which are consistent with previous work for carbonaceous chondrites (positive odd-MIF) and ordinary chondrites (no MIF), and demonstrate that some enstatite chondrites exhibit positive odd-MIF, similar to carbonaceous chondrites. The terrestrial igneous rocks fall within the range of chondritic compositions for both MIF and MDF. Given the fact that planetary differentiation (core formation, evaporation) would contribute to Hg loss from the silicate portion of Earth and would likely fractionate Hg isotopes from chondritic compositions, we suggest that the budget of the mantle Hg is dominated by late accretion of chondritic materials to Earth, as also suggested for other volatile chalcophile elements (S, Se, Te). Considering the Hg isotopic signatures, materials with compositions similar to CO chondrites or ordinary chondrites are the most likely late accretion source candidates. Finally, eucrite meteorites, which are highly depleted in volatile elements, are isotopically heavier than chondrites and exhibit negative odd-MIF. The origin of volatile depletion in eucrites has been vigorously debated. We show that Δ^{199}Hg versus Δ^{201}Hg relationships point toward an equilibrium nuclear field shift effect, suggesting that volatile loss occurred during a magma ocean phase at the surface of the eucrite parent body, likely the asteroid 4-Vesta.

1. Introduction

One of the most fundamental differences amongst the terrestrial planetary bodies, including Earth, Mars, the Moon and differentiated asteroids, is the general depletion of volatile elements in their silicate fraction compared to undifferentiated meteorites (chondrites) (e.g. Palme et al., 2014. In particular, moderately volatile elements show a depletion pattern that is broadly cor-

* Corresponding author at: State Key Laboratory of Geological Processes and Mineral Resources, School of Earth Sciences, China University of Geosciences, Wuhan 430074, China.
E-mail addresses: moynier@ipgp.fr (F. Moynier), jbchen@tju.edu.cn (J. Chen).

https://doi.org/10.1016/j.epsl.2020.116544
0012-821X/

related with decreasing mass in terrestrial planetary bodies, and is generally interpreted as the consequence of volatility processes, either in the solar nebula or during planetary formation and evolution (e.g. O'Neill and Palme, 2008; Day and Moynier, 2014; Siebert et al., 2018; Braukmüller et al., 2019). Because isotopes of moderately volatile elements are fractionated during volatility-driven processes and planetary differentiation, the study of their isotopic compositions has been key in testing the inventories of these elements in planets and the consequences that volatile loss has for planetary evolution (e.g. Poitrasson et al., 2004; Wombacher et al., 2008; Sharp et al., 2010; Paniello et al., 2012a, 2012b; Day and Moynier, 2014; Boyce et al., 2015; Vollstaedt et al., 2016; Wang and Jacobsen, 2016; Creech and Moynier, 2019; Varas-Reus et al., 2019; Wang et al., 2019).

Among the moderately volatile elements (MVE), mercury is of particular significance as it is by far the most volatile (temperature of 50% condensation, $T_c = 252$ K) and likely behaves more like a highly volatile element (e.g. Meier et al., 2016). Springmann et al. (2019) showed that Hg is the most labile metal in meteorites and could be used to track the thermal metamorphic history in meteorites. However, Hg Isotope systematics have not been extensively reported for investigating planetary differentiation, largely due to complications in measurement. Mercury has seven stable isotopes: ^{196}Hg (0.16%), ^{198}Hg (10.04%), ^{199}Hg (16.94%), ^{200}Hg (23.14%), ^{201}Hg (13.17%), ^{202}Hg (29.73%), and ^{204}Hg (6.83%), and large mass-dependent and mass-independent isotopic fractionations (e.g. Blum et al., 2014) have been reported.

Development of high-precision Hg isotopic measurements has been motivated by the toxicity of Hg, in particular due to the accumulation of methyl-mercury in seawater and fish, and the application of Hg isotopes as tracers of pollution (e.g. Bergquist and Blum, 2007; Blum et al., 2014; Foucher and Hintelmann, 2006). In particular, it has been shown that Hg isotopes are fractionated by several identified mechanisms, including mass-dependent isotopic fractionation (MDF), and, more specific to Hg, large (over 1‰) mass-independent isotopic fractionation (MIF) of odd isotopes (odd-MIF) due to magnetic isotope effects (MIE) (e.g. Bergquist and Blum, 2007) or the nuclear field shift effect (NFSE) (Estrade et al., 2009). Mercury is also subject to MIF of even isotopes (even-MIF), most probably due to photo-chemical reactions (Chen et al., 2012). The broad utility and behavior of Hg isotopes has therefore led to proliferation of these measurements in surficial environments (e.g. Bergquist and Blum, 2007; Blum et al., 2013; Chen et al., 2012; Estrade et al., 2010; Foucher and Hintelmann, 2006; Sherman et al., 2010; Sonke et al., 2010). In contrast, high temperature applications of Hg isotopes are less-well established (Lauretta et al., 2001; Zambardi et al., 2009; Wiederhold and Schönbächler, 2015; Meier et al., 2016).

The pioneering work of Lauretta et al. (2001) suggested that the carbonaceous chondrites, Allende and Murchison, have Hg isotopic compositions similar to the terrestrial Almadèn mine cinnabar (UM-Almadèn) within 0.5‰. More recently, Meier et al. (2016) analyzed the Hg elemental abundance and isotopic composition of a larger set of meteorites and found surprisingly large isotopic variations of both MDF (expressed as δ^{202}Hg, the permil deviation of the ^{202}Hg/^{198}Hg ratio compared to the NIST SRM 3133 standard) and odd-MIF compared to that which was originally identified in Lauretta et al. (2001), consistent with earlier data reported in an abstract (Wiederhold and Schönbächler, 2015). This work shows that carbonaceous chondrites exhibit odd-MIF signatures while non-carbonaceous chondrites do not. However, these measurements were limited to a few LL ordinary chondrites and a single L ordinary chondrite, and no enstatite chondrites were examined for a MIF signature. In addition, Meier et al. (2016) argued that the Hg isotopic composition of chondrites is lighter (δ^{202}Hg down to −7.13‰) than the known terrestrial Hg composition (terrestrial δ^{202}Hg is estimated to be -0.68 ± 0.45 (1sd), based on sedimentary rocks; Blum et al., 2014).

Of relevance is that potential isotopic differences between the bulk silicate Earth (BSE) and chondrites could be used to trace the origin of mantle mercury. Mercury exhibits a deficit in the silicate portion of the Earth relative to CI chondrites: due to its strongly chalcophile behavior, most of the original terrestrial Hg may have been partitioned into Earth's core or, because of its high volatility, it may have also been lost by evaporation during planetary accretion, as suggested for other chalcophile MVE (S, Te and Se; Steenstra et al., 2017; Wang and Becker, 2013). Thus, the present-day Hg content of the mantle may represent late accretion addition as suggested for the highly siderophile elements (HSE) (e.g. Day et al., 2007, 2016; Fischer-Gödde et al., 2020), and possibly highly volatile elements (Marty, 2012), as well as Se, Te and S (Wang and Becker, 2013; Varas-Reus et al., 2019). In this case, Earth's mantle would be expected to have a chondritic composition. On the other hand, if mantle Hg was preserved during Earth's formation, it would be expected that Hg isotopes would be isotopically fractionated by either, or both, core formation and volatilization, as observed for other chalcophile MVE (e.g. Cu, Savage et al., 2015). In addition, the fact that some meteorites exhibit MIF of Hg isotopic ratios could potentially be used as an additional tool to track the origin of Earth's Hg, as the relation between Δ^{201}Hg and Δ^{199}Hg depends on the specific mechanism of isotopic fractionation (Estrade et al., 2009; Ghosh et al., 2013).

Available Hg isotopic data for igneous rocks include some samples from the California coast range, including ophiolitic and volcanic rocks, which have experienced significant alteration and crustal assimilation, respectively (Smith et al., 2009, Hammersley and Depaolo, 2006). More recently, Geng et al. (2018) reported data for four geostandards, including two basalts, suggesting isotopic variability among terrestrial igneous rocks. Due to the limited Hg isotopic data for well-preserved mantle or mantle-derived rocks, the terrestrial composition sometimes includes sedimentary rocks. In order to establish the utility of Hg isotopes for cosmochemistry and geochemistry it is therefore critical to analyze more mantle-derived rocks to establish its composition. Furthermore, previous studies on meteoritic compositions report the full Hg isotopic composition for only 11 chondrites. Some important meteoritic groups such as enstatite chondrites, which are the closest to BSE in terms of isotopic composition (e.g. Javoy et al., 2010) have not been examined. This omission is important given the Hg isotopic variations observed in Meier et al. (2016).

Here, we report the Hg isotopic composition of chondrites including four carbonaceous chondrites, five ordinary chondrites, four enstatite chondrites and eight terrestrial igneous rocks, which comprise basalts, trachytes and granites, in order to estimate the average terrestrial composition and to test the origin of mantle Hg. Since there are very few Hg isotopic data of terrestrial igneous rocks, we have chosen to report data for widely available and well characterized geostandards from the USGS (USA) and the CRPG (France). We also report isotopic data for a basaltic eucrite meteorite, considered to derive from the asteroid 4-Vesta or vestoids, which is highly volatile depleted. Our results confirm previous isotopic data for meteorites, expand the data to enstatite chondrites, and show that igneous rocks are isotopically lighter than sedimentary rocks. Therefore, previous estimates for rock composition, which relied on sedimentary rocks, cannot be used as the terrestrial composition. We discuss the origin of the terrestrial and vestan Hg in light of the mass-dependent and mass-independent fractionations of Hg isotopes.

2. Samples and method

2.1. Sample descriptions

Meteorite samples were chosen that are representative of most carbonaceous chondrite (CC: CI, CM, CO, CV), ordinary chondrite (OC: H, LL), and enstatite chondrite (EC: EH, EL) groups. We also analyzed a single eucrite (Dhofar 007), a polymict breccia with evidence for meteoritic contamination from highly siderophile element abundances (Dale et al., 2012). All the chondrite samples are falls. The CC are Orgueil (CI1), Allende (CV3), Murchison (CM2) and Felix (CO3). The OC are Allegan (H5), Kernouve (H6), Olivenza (LL5), Tuxtuac (LL5) and St Severin (LL6). The EC are Abee (EH4), Indarch (EH4) and Hvittis (EL6). Among these meteorites we selected some samples to perform several full replicates, either from the same homogeneous powder (Orgueil 1-3, Indarch 2-4, Tuxtuac 1-2), or from different chips (Allegan 1-2, Tuxtuac 2, Allende 1-3, Murchison 1-2, and Indarch 1) to test for the reproducibility of the full procedure and assess sample heterogeneity (cf. Meier et al., 2016).

The terrestrial samples consist of a variety of mafic to felsic standard rocks, including, USGS BIR-1 (basalt, Iceland) and SARM (service d'analyse des roches et des minéraux, Nancy, France) BE-N (basalt, France), ISH-G (trachyte, Italy), MDO-G (trachyte, France), GA (granite, France), AC-E (granite, UK), GH (granite, Algeria), and a trachyte sample from the Bouvet hot spot, southern Atlantic Ocean (BV2, O'Nions et al., 1977). We selected magmatic rocks over peridotites to identify the Hg isotopic composition of terrestrial igneous rocks for two reasons: 1) Since Hg is a moderately incompatible element (Canil et al., 2015), the Hg content of peridotites is much lower than in magmatic rocks making them even more challenging to analyze and; 2) Hg is highly heterogeneous in peridotites, making it sensitive to nuggets effects, as well as metasomatic processes, while it is more homogeneous in magmatic rocks (Canil et al., 2015). In addition, we analyzed the isotopic composition of the UM (Univeristy of Michigan) Almedén cinnabar standard, which is a sample solution provided by the University of Michigan and that is widely used as an external standard for inter-laboratory comparison.

2.2. Reagents and materials

For all experiments, MilliQ H_2O (18.2 MΩ) and double-distilled concentrated HCl and HNO_3 were used, along with certain analytical grade reagents ($NH_2OH{\cdot}HCl$, $SnCl_2$, KBr, $KBrO_3$) from Sigma-Aldrich (USA). A 0.2 M BrCl solution was made by mixing concentrated HCl with preheated (250 °C, 12 h) KBr and $KBrO_3$ powders. NIST SRM 3133 Hg and NIST SRM 3177 Hg were chosen as isotopic standard solutions. NIST SRM 997 Tl was employed for instrumental mass bias correction (Chen et al., 2010). UM-Almadén Hg and two certified reference materials (CRM) GBW07311 (stream sediments) and GBW07405 (yellow-red soil) (National Center for Standard Materials, Beijing, China) were used to evaluate the instrument stability and pre-treatment efficiency, and measured regularly during analytical sessions. All borosilicate glass materials (bottles, impingers, elbow-shaped tubes, sample quartz tubes) were soaked in 1% BrCl + 15% HNO_3 solution for 24 hrs and rinsed with MilliQ H_2O, then heated at 500 °C for 3 hrs before their use to remove traces of Hg. Teflon materials were similarly acid-cleaned and then air-dried.

2.3. Mercury concentration measurement

Mercury concentrations in meteorite and rock samples were measured using a Lumex Hg analyzer RA 915F equipped with a pyrolysis attachment PYRO-915+. The instrument detection limit of Hg is 0.5 ng/g. CRM GBW07311 and CRM GBW07405 were used to verify the data accuracy, with the determined concentration within ±10% of their certified Hg values. The Hg concentrations of samples were compared with those obtained from the multi-collector inductively-coupled-plasma mass-spectrometer (MC-ICP-MS) to evaluate and guarantee the Hg recovery (of 95 ± 11%; 2SD) for all samples except for BV2 (82%), during the treatment (double combustions and trapping) and prior to isotope analysis (see below). The double combustion system consisted of a furnace quartz tube (25 mm OD, 22 mm ID, 1.0 m length) placed in two combustion tube furnaces (Lindberg/Blue M Mini-Mite, Thermo Ltd., USA). The solid samples were placed in the quartz tube and Hg in the samples was completely released by combustion. The first combustion furnace was set to rapidly raise temperature from ambient to 950 °C to release Hg, followed by a second decomposition furnace for maintaining constant temperature at 1,000 °C. The combustion products (gaseous Hg) were carried by Hg-free O_2 gas into the 5 ml trapping solution composed of 2:4:9 ratio of 10 M HCl, 15 M HNO_3 and Milli-Q water, which capture all combustion-released Hg. The detailed description of the double combustion system could be found in Huang et al. (2015).

2.4. Mercury isotope ratio analysis

An improved combustion and trapping method described by Huang et al. (2015) was adopted in this study for the purification and pre-concentration of Hg from solid samples. Considering the Hg contents of some meteorite samples were less than 10 ng, we optimized the acid trapping device by narrowing the internal diameter size of the borosilicate glass impinger. Each weighed sample was step-combusted in dual-stage furnaces and the combustion products were carried by Hg-free O_2 gas into a 3 mL 40% (v/v, $2HNO_3$/1HCl) acid-trapping solution. The trapping device was rinsed with 3 mL MilliQ H_2O. An aliquot of 200 µL of 0.2 M BrCl was added to stabilize the Hg^{2+}. The final trapping solutions were transferred to 40 mL pre-cleaned (at 500 °C for 3 hrs) borosilicate glass bottles and stored at 4 °C for the subsequent Hg concentration and isotope measurement. The two certified reference materials CRM GBW07311 (Hg = 72 ± 9 ng/g) and CRM GBW07405 (Hg = 290 ± 30 ng/g) were processed in the same way, which yielded Hg recoveries of 98 ± 4% (2SD, $n = 6$) and 99 ± 8% (2SD, $n = 16$) respectively.

Mercury isotopic analysis was carried out using an MC-ICP-MS (Nu Plasma 3D, Nu Instruments, UK) equipped with a home-made continuous flow cold vapor generation system at the Institute of Surface-Earth System Science, Tianjin University, following the same setup as described in previous studies (Chen et al., 2010; Huang et al., 2015; Yuan et al., 2018; Zhang et al., 2020). Briefly, the Hg(0) vapor was generated via online reduction of $SnCl_2$ (3%) solution. The Tl aerosol produced from the Aridus II nebulizer was simultaneously introduced into the plasma with Hg(0). The instrumental mass bias was corrected by an internal NIST SRM 997 Tl standard using the standard-sample bracketing method. The sample solutions were introduced at 0.7 mL/min, which gave an instrumental sensitivity of 2.5 V on ^{202}Hg for 1 ng/mL Hg solution. Mercury concentrations of bracketing standards NIST SRM 3133 and secondary standard UM-Almadén were matched to the sample solutions within 10%. All samples were analyzed in three blocks with 33 cycles for each and within 10 min washout time in between samples to ensure the blank levels were <0.2% of the preceding sample signals.

The data for mass-dependent fractionation of Hg isotopes is reported as $\delta^x Hg$, the permil deviation of the $^xHg/^{198}Hg$ ratio relative to the NIST-3133 standard, and is defined as:

Table 1
Mercury isotopic and elemental composition the meteoritic samples analyzed in this study and in Meier et al. (2016). The full data table can be found in supplementary materials (Table S2).

Samples		Hg (ng/g)	δ^{202}Hg	2SD	Δ^{199}Hg	2SD	Δ^{200}Hg	2SD	Δ^{201}Hg	2SD	Δ^{204}Hg	2SD
Orgueil	CI1	23380	−3.85	0.04	0.19	0.00	0.01	0.02	0.09	0.04	−0.03	0.03
Orgueil	CI1	23380	−4.04	0.04	0.22	0.00	0.04	0.02	0.11	0.04	−0.01	0.03
Orgueil	CI1	23380	−4.03	0.04	0.20	0.00	0.02	0.02	0.12	0.04	0.00	0.03
Orgueil Meier	CI1	13600	−3.74	0.18	0.26	0.03	0.06	0.04	0.16	0.07	−0.03	0.20
Tagish Lake Meier	C2	71	−3.57	0.20	0.25	0.05	0.06	0.03	0.14	0.02	0.00	0.09
Murchison-1	CM2	408	−2.79	0.06	0.04	0.03	0.02	0.03	−0.02	0.05	−0.08	0.03
Murchison-2	CM2	221	−1.62	0.08	0.26	0.03	0.09	0.03	0.07	0.05	−0.16	0.09
Murchison Meier	CM2	2570	−1.29	0.65	0.15	0.10	0.01	0.01	0.06	0.04		
Paris Meier	CM2	11800	−3.38	0.18	0.31	0.06	0.01	0.08	0.14	0.05	−0.02	0.09
Felix	CO3.2	2832	−1.01	0.08	−0.02	0.03	0.00	0.03	−0.03	0.05	0.07	0.09
Kainsaz Meier	CO3.2	267	−7.13	0.03	0.10	0.10	0.03	0.11	0.07	0.12	−0.02	0.09
Allende-1	CV2	102	−3.14	0.06	0.01	0.03	0.01	0.03	0.01	0.05	−0.01	0.03
Allende-2	CV2	127	−5.75	0.08	0.14	0.02	0.04	0.03	0.11	0.03	−0.01	0.06
Allende-3	CV2	475	−2.08	0.08	0.05	0.03	0.01	0.03	0.02	0.05	−0.03	0.09
Allende Meier	CV2	39	−3.66	0.57	0.25	0.13	0.07	0.04	0.08	0.22	0.04	0.01
Karoonda Meier	CK4	401	−2.46	0.12	−0.07	0.04	0.02	0.04	−0.09	0.09	−0.04	0.01
Bencubbin silicates Meier	CB	202	−4.2	0.49	0.06	0.06	−0.02	0.04	0.06	0.06	0.00	0.04
Abee	EH4	190	−3.58	0.08	0.08	0.03	0.00	0.03	0.06	0.05	0.04	0.09
Indarch-1	EH4	69	−2.60	0.21	0.06	0.03	−0.02	0.08	0.07	0.02	0.06	0.04
Indarch-2	EH4	204	−3.85	0.10	0.22	0.08	0.01	0.01	0.16	0.09	−0.02	0.04
Indarch-3	EH4	204	−3.87	0.10	0.22	0.08	0.01	0.01	0.16	0.09	−0.03	0.04
Indarch-4	EH4	204	−3.78	0.10	0.15	0.08	0.02	0.01	0.08	0.09	0.01	0.04
Hvittis	EL6	652	−3.01	0.06	0.03	0.03	0.01	0.03	−0.01	0.05	0.02	0.03
Allegan-1	H5	1822	−2.39	0.06	0.02	0.03	0.03	0.03	−0.03	0.05	−0.02	0.03
Allegan-2	H5	2857	−2.28	0.03	0.14	0.03	0.02	0.03	0.08	0.04	0.00	0.01
Kernouve	H6	445	−2.18	0.06	−0.02	0.03	0.00	0.03	−0.03	0.05	−0.02	0.03
Olivenza	LL5	305	−2.30	0.06	−0.03	0.03	0.03	0.03	−0.08	0.05	0.02	0.03
St Severin	LL6	335	−2.70	0.06	0.01	0.03	0.02	0.03	−0.02	0.05	−0.01	0.03
Tuxtuac-1	LL5	165	−1.71	0.06	−0.03	0.03	0.00	0.03	−0.02	0.05	−0.01	0.03
Tuxtuac-2	LL5	165	−1.77	0.06	0.00	0.02	0.01	0.01	−0.04	0.00	0.01	0.01
Tuxtuac-3	LL5	174	−1.73	0.06	−0.02	0.02	0.01	0.01	−0.04	0.00	0.00	0.01
Mezo Madaras Meier	L3.7	3150	−1.19	0.23	−0.06	0.02	−0.03	0.04	−0.1	0.08	−0.40	0.24
Mocs Meier	L6	965	−2.4	0.79	0.06	0.05	0.01	0.03	−.010	0.07		
Dhofar 007	Euc	5	0.00	0.08	−0.26	0.03	−0.04	0.03	−0.12	0.05	0.16	0.09
Millbillillie Meier	Euc	28	−0.73	0.31	−0.26	0.04	−0.08	0.07	−0.13	0.04	−0.2	0.06

$$\delta^{x}\mathrm{Hg}(‰) = \left[\left({}^{x}\mathrm{Hg}/{}^{198}\mathrm{Hg}\right)\mathrm{sample}/\left({}^{x}\mathrm{Hg}/{}^{198}\mathrm{Hg}\right)_{\mathrm{NIST\ SRM\ 3133}} - 1\right] \times 1000 \quad (1)$$

where x refers to the mass of each isotope between 199 and 202 amu. By convention, δ^{202}Hg is used for the discussion of MDF variations and as the reference ratio with which to calculate the mass-independent fractionation MIF. The MIF data are defined as the deviation of the δ^{x}Hg from the theoretical value estimated from the δ^{202}Hg based on kinetic isotopic fractionation (e.g. Blum and Johnson, 2017):

$$\Delta^{x}\mathrm{Hg}(‰) = \delta^{x}\mathrm{Hg}(‰) - \beta^{x} \times \delta^{202}\mathrm{Hg} \quad (2)$$

where the mass dependent scaling factor β^{x} is 0.2520, 0.5024 and 0.7520 for ^{199}Hg, ^{200}Hg and ^{201}Hg, respectively.

During the analysis session, repeated measurements gave average values of −0.53 ± 0.07‰, 0.00 ± 0.03‰, 0.01 ± 0.03‰ and −0.03 ± 0.05‰ for δ^{202}Hg, Δ^{199}Hg, Δ^{200}Hg and Δ^{201}Hg of UM-Almadén Hg (2SD, $n = 21$), and −1.75 ± 0.05‰, −0.35 ± 0.03‰, 0.00 ± 0.05‰ and −0.32 ± 0.04‰ for those of CRM GBW07405 (2SD, $n = 5$), respectively. All values were consistent with previous results (Chen et al., 2010; Huang et al., 2019; Zhang et al., 2020). The 2SD of UM-Almadén with δ^{202}Hg, Δ^{199}Hg, Δ^{200}Hg and Δ^{201}Hg of respectively 0.08‰, 0.03‰, 0.03‰, 0.05‰ represent the typical analytical uncertainties of our samples. Errors are reported as twice the standard deviation from the replicate measurements of the same solution (generally measured two times).

3. Results

Because of the low Hg content of some samples (in particular the eucrite meteorite), we performed sensitivity tests using the UM-Almadén solution. We ran the solution with concentrations between 1 ppb (the concentration used for most samples) down to 0.22 ppb (Table S1). At 0.22 ppb, which corresponds to ∼0.2 ng of Hg processed, the accuracy and precision of both MDF and of the MIF are not influenced by the reduction of the signal, where ^{202}Hg drops from ∼2 V to 0.6 V (Table S1). All data obtained on the UM-Almadén samples are consistent with literature values (Blum and Johnson, 2017).

Isotopic and concentration data for the meteoritic and terrestrial samples are reported in Tables 1 and 2 and in Table S2. Data are reported using the traditional notation relative to the NIST-3133 standard (see Blum and Johnson, 2017) and the MIF are calculated as described above. Replicate measurements of meteoritic samples from the same powder return values (both δ^{202}Hg and MIF) consistent within error confirming the overall reproducibility of the full analytical procedure (Table 1). On the other hand, different chips of the same meteorite have more variable δ^{202}Hg while MIF stays consistent. These isotopic variations were observed by Meier et al. (2016) and may represent sample heterogeneity within meteoritic samples.

The isotopic compositions of chondrites are in good agreement with those reported by Meier et al. (2016) for the same samples that we analyzed (i.e. for Orgueil, Allende, Murchison), with gen-

Table 2
Mercury isotopic and elemental composition of the terrestrial samples analyzed in this study. The full data table can be found in supplementary materials (Table S2).

Samples		Hg (ng/g)	δ^{202}Hg	2SD	Δ^{199}Hg	2SD	Δ^{200}Hg	2SD	Δ^{201}Hg	2SD	Δ^{204}Hg	2SD
BE-N	basalt	14	−3.08	0.08	0.00	0.03	0.01	0.03	−0.02	0.05	−0.01	0.09
BIR-1	basalt	3	−2.42	0.08	0.04	0.03	0.08	0.03	0.01	0.05	−0.04	0.09
GA	granite	42	−4.40	0.08	0.02	0.03	0.00	0.03	0.01	0.05	0.01	0.09
GH	granite	8	−2.90	0.08	−0.04	0.03	0.01	0.03	−0.07	0.05	0.03	0.09
GIT ACE-E	granite	6	−3.56	0.08	−0.05	0.03	−0.02	0.03	−0.01	0.05	−0.01	0.09
GIT MDO-G	trachyte	7	−2.73	0.08	−0.05	0.03	0.05	0.03	0.01	0.05	−0.04	0.09
Bouvet BV2	trachyte	4	−2.35	0.08	−0.03	0.03	−0.01	0.03	−0.06	0.05	0.05	0.09
ISH-G	trachyte	8	−4.95	0.08	0.06	0.03	0.00	0.03	0.02	0.05	−0.05	0.09

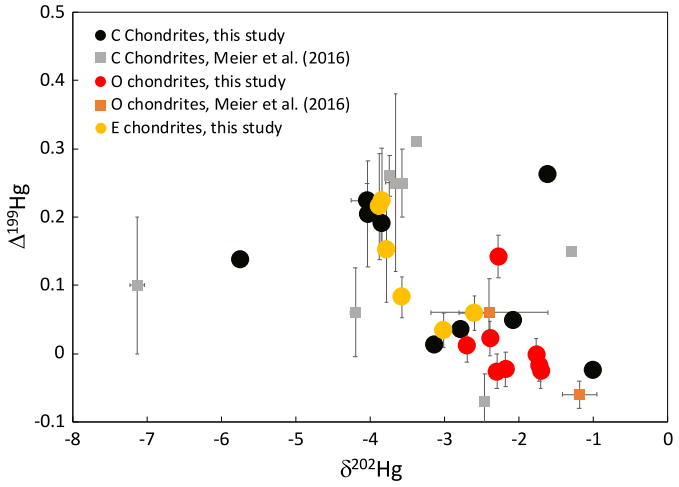

Fig. 1. Δ^{199}Hg against δ^{202}Hg for chondrites from this study and Meier et al. (2016). (For interpretation of the colors in the figure(s), the reader is referred to the web version of this article.)

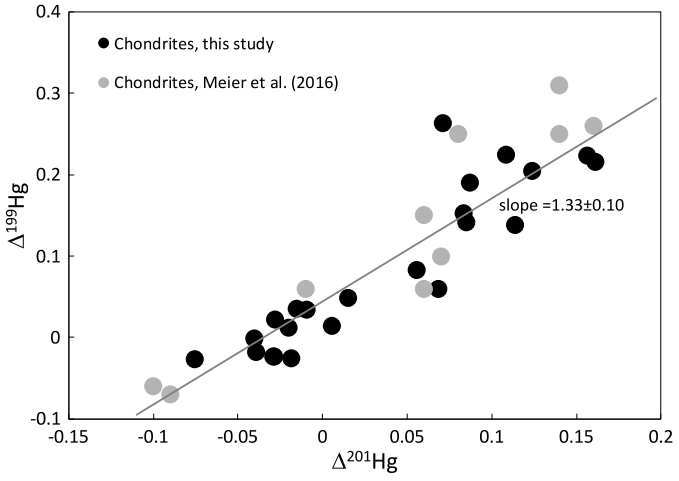

Fig. 2. Δ^{199}Hg against Δ^{201}Hg. The slope of 1.33 ± 0.10 corresponds to what is predicted for evaporation under kinetic conditions (slope ~1.2, Estrade et al., 2009).

erally positive odd-MIF and negative δ^{202}Hg (Fig. 1). The data are in particularly good agreement for Orgueil (δ^{202}Hg = −3.74 ± 0.18, Δ^{199}Hg = 0.26 ± 0.03, Δ^{201}Hg = 0.16 ± 0.07 in Meier et al. (2016) versus δ^{202}Hg = −3.97 ± 0.22, Δ^{199}Hg = 0.21 ± 0.03, Δ^{201}Hg = 0.11 ± 0.04 for this study). For Allende and Murchison, the odd-MIF is smaller in our study, but with the same general positive shift (Fig. 2) and no meteorites exhibit even-MIF. For the CO chondrites, while we have no samples in common between our data and that of Meier et al. (2016), Felix and Kainsaz, respectively, are the only CCs that return MIF indistinguishable from zero. The results for δ^{202}Hg are more variable, and the relatively small differences between our study and Meier et al. (2016) may result from sample heterogeneity.

The five ordinary chondrites have Hg isotopic compositions in the range observed previously (Meier et al., 2016; Wiederhold and Schönbächler, 2015). The δ^{202}Hg is less variable than in CC, and falls between −2.70 and −1.70. As observed by Meier et al. (2016) most OC do not exhibit any odd-MIF, but here we find one instance (Allegan) that shows slightly positive MIF (Δ^{199}Hg = 0.14 ± 0.03, Δ^{201}Hg = 0.08 ± 0.04).

Both EH and EL chondrites show limited variations in the δ^{202}Hg values (between −4.00 and −3.00), as also shown for the OC. The two EH exhibit clear positive MIF while the EL6 sample shows no MIF effect (Table 1).

As previously observed (Meier et al., 2016; Wiederhold and Schönbächler, 2015) isotopic and elemental abundances of Hg vary within single chondrite samples (Table 1). The elemental variations within a single chondrite have been interpreted to be caused by nuggets effects of Hg carriers, most probably HgS (Meier et al., 2016; Caillet Komorowski et al., 2012). For Orgueil and Murchison, we find Hg concentrations close to those obtained by Meier et al. (2016), while for Allende our two different sample splits each have slightly different concentrations than those reported previously. Meier et al. (2016) performed heating experiments on Orgueil and Mezo-Madaras (OC, L3.7) to desorb possible terrestrial contamination and demonstrated limited terrestrial contamination, at least for meteorite falls, a reason why we only selected falls of chondrite meteorites.

The eucrite Dhofar 007 is highly depleted (by a >factor 100) in Hg compared to chondrites, and has δ^{202}Hg higher (−1.16 ± 0.08) than most chondrites and negative odd-MIF (Δ^{199}Hg = −0.26 ± 0.03, Δ^{201}Hg = −0.13 ± 0.05) (Table 1). This is consistent with the data from Meier et al. (2016) for another eucrite, Millbillillie (δ^{202}Hg = −0.73 ± 0.31, Δ^{199}Hg = −0.26 ± 0.03, Δ^{201}Hg = −0.13 ± 0.04), and the data of Wiederhold and Schönbächler (2015) for Pasamonte (δ^{202}Hg ~−1.5) and Bouvante (δ^{202}Hg ~0) (see Fig. 3). While our eucrite samples (as well as Bouvante) are not observed fall meteorites they give consistent results with Millbillillie and Pasamonte which are two observed falls, suggesting limited effect of terrestrial loss or contamination on their Hg isotopic composition.

The terrestrial igneous rock samples show variable δ^{202}Hg, from −4.95 to −2.35, with no systematic difference between felsic and mafic rocks (Table 2). The basalts have δ^{202}Hg between −3.08 and −2.42, the trachytes between −4.95 and −2.35, and the granites between −4.40 and −2.90. The terrestrial samples exhibit small odd-MIF (Δ^{199}Hg between −0.05±0.03 and +0.06±0.03), that is slightly correlated (P value = 0.08) with the MDF (Figs. 4 and 5). The terrestrial samples do not exhibit even-MIF.

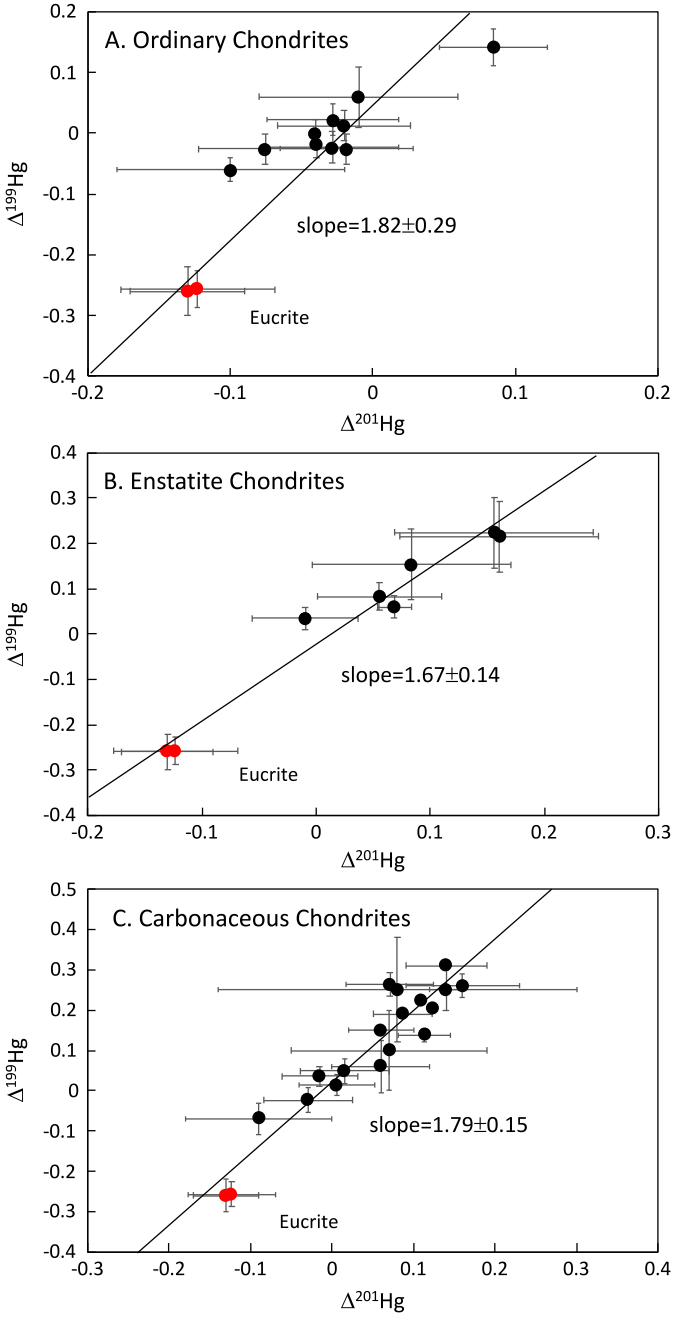

Fig. 3. Δ^{199}Hg against Δ^{201}Hg for the eucrite meteorites (red dots) together with ordinary chondrites (A), enstatite chondrites (B), and carbonaceous chondrites (C). The slopes comprised between 1.67 and 1.82 correspond to what is predicted for evaporation under equilibrium conditions.

4. Discussion

4.1. Isotopic variations preserved in chondrites controlled by kinetic evaporation

As previously observed (Wiederhold and Schönbächler, 2015; Meier et al., 2016;), chondrites exhibit large MDF with no systematic variations between chondrite groups nor correlations with Hg abundance (Fig. 6). The behavior of Hg isotopes is clearly different from other moderately volatile elements such as Zn (Luck et al., 2005; Pringle et al., 2017) or Rb (Pringle and Moynier, 2017), which show systematic variations in chondrite meteorites. The MDF and odd-MIF variations observed in carbonaceous chondrites and ordinary chondrites have already been discussed in Meier et al.

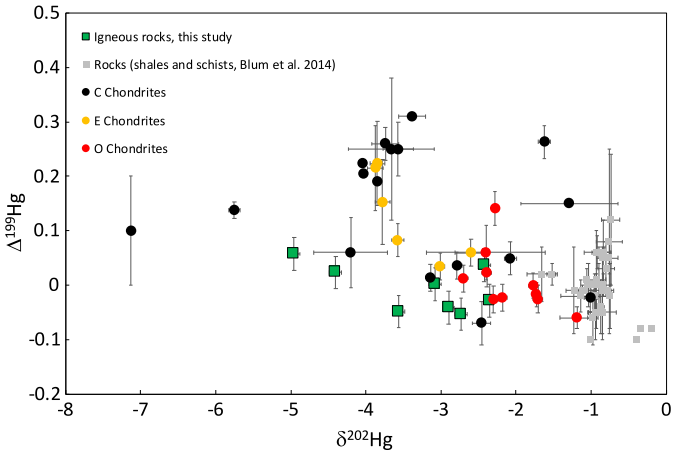

Fig. 4. Δ^{199}Hg against δ^{202}Hg for terrestrial and meteoritic samples. Terrestrial igneous rocks are isotopically heavier than shales and schists that had previously been used as representing the composition of the Earth (data from Blum et al., 2014). The igneous rocks fall within the range defined by chondrites.

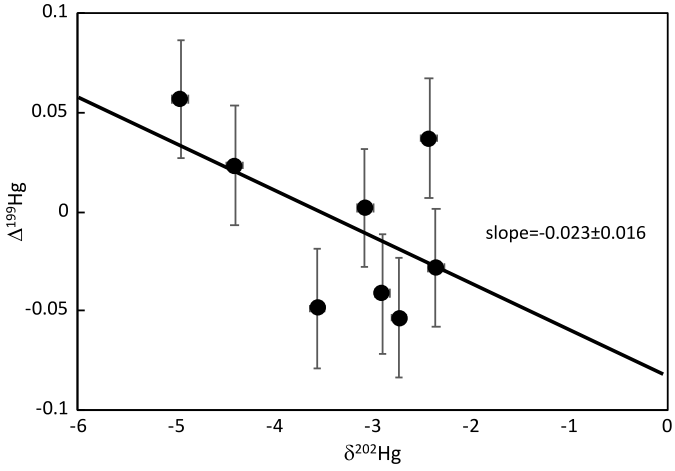

Fig. 5. Δ^{199}Hg against δ^{202}Hg for the terrestrial igneous rocks. The weak correlation with a slope of −0.023 is consistent with evaporation under kinetic conditions, possibly corresponding to volatile loss during magma degassing.

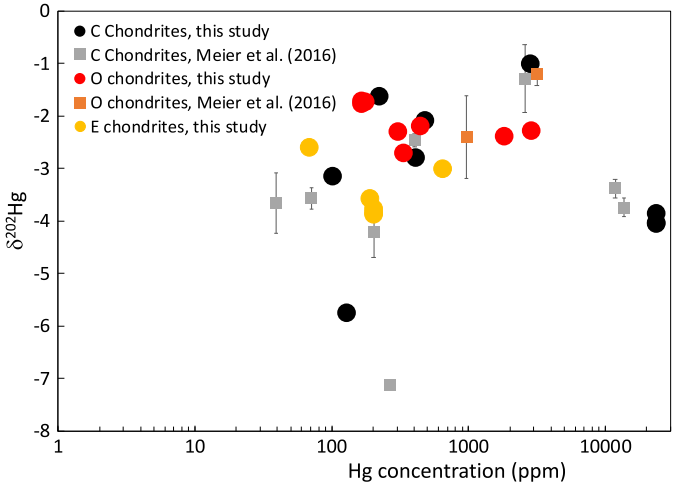

Fig. 6. δ^{202}Hg against Hg concentration for chondrites, including data from Meier et al. (2016) and this study. Mercury isotopic composition does not correlate with Hg concentration.

(2016). While we do not report ^{196}Hg due to its low natural isotopic abundance, Meier et al. (2016) has shown that chondrites do not exhibit nucleosynthetic ^{196}Hg anomalies, suggesting that other odd isotope (^{199}Hg and ^{201}Hg) variations are not due to nucleosynthetic effects either, but rather are attributed to MIF.

Previous studies have reported that the Δ^{199}Hg/Δ^{201}Hg ratio provides specific information on the processes, as variable mechanisms (e.g. nuclear field shift effect versus magnetic isotope effect) would induce different isotopic ratios (Blum et al., 2014 and references therein). Meier et al. (2016) focused the discussion on the Δ^{199}Hg versus Δ^{201}Hg correlation and the meaning of the slope. It has been shown that during a given process, e.g. evaporation/condensation, the slope in this diagram depends on the degree of equilibrium of the reaction, as different mechanisms will be acting on the process (nuclear field shift effect versus magnetic isotope effect). For example, during kinetic evaporation, based on evaporation experiments, the slope is estimated to be ~1.2 (Estrade et al., 2009), while under equilibrium condition the slope has been found to be higher, at 1.59 ± 0.05 (2 standard error, 2se) (Ghosh et al., 2013) to 2.0 ± 0.6 (2se) (Estrade et al., 2009). As a caveat, it should be noted that the kinetic evaporation experiments of Estrade et al. (2009) were conducted under low temperature (<100 °C) and we assume here that the slope holds at higher temperature. Furthermore, these experiments were carried out by evaporating pure Hg under vacuum, but the condition of degassing on the meteorite parent body would have been different, which could also affect the value of the slope. High temperature volatilization experiments under various conditions will therefore be necessary to further confirm the evaporation conditions.

Including all the chondritic data, we obtain a slope of 1.33 ± 0.10 (1sd) in a Δ^{199}Hg versus Δ^{201}Hg diagram (Fig. 2). This slope is similar to that obtained by Meier et al. (2016), while including almost three times more data. This suggests a process dominated by kinetic evaporation/condensation (slope of ~1.2), most probably during degassing on the meteoritic parent bodies. The MDF of the chondrites is therefore variable ($-7 < \delta^{202}$Hg < -1) and it is thus likely controlled by the evaporation/condensation process. We also show that EH chondrites exhibit a positive odd-MIF (Fig. 1).

4.2. Heavy isotopes enrichment in eucrites reflect evaporation under an equilibrium regime

The general heavy isotope enrichment (high δ^{202}Hg values) for eucrites (our datum, Meier et al., 2016; Wiederhold and Schönbächler, 2015) (Fig. 3), likely originating from the asteroid 4-Vesta, is consistent with light isotope loss during volatilization of Hg, as previously observed for other moderately volatile elements (Zn, Rb, K, Cd; Wombacher et al., 2008; Paniello et al., 2012b; Pringle and Moynier, 2017; Tian et al., 2019). This heavy isotope enrichment is generally interpreted to reflect volatile loss due to evaporation during the history of Vesta. The major unanswered question is whether this process happens during the emplacement of the lavas at the surface of the asteroid or following impacts (most likely a kinetic effect), or during the degassing of a magma ocean (possibly an equilibrium process). Based on an apparent small enrichment in the lighter isotopes of Cr in HED (group of meteorites, likely from Vesta) meteorites, Zhu et al. (2019) suggested that Vesta lost isotopically heavy Cr isotopes during degassing, reflecting equilibrium isotopic fractionation rather than kinetic fractionation. Given that the relation between Δ^{199}Hg and Δ^{201}Hg is different between kinetic effects controlled by magnetic isotope effects (slope of ~1.2, Estrade et al., 2009) and equilibrium fractionation due to the nuclear field shift effect (slope between 1.59 ± 0.05, Ghosh et al. (2013) and 2.0 ± 0.6 Estrade et al. (2009)), it is possible to test the degree of equilibrium of the fractionation. As we show below, whatever chondrite type is used to represent the HED parent body starting materials does not affect the final results. While the HED starting material composition is not known, ordinary chondrites possess the closest Cr and Ti isotopic composition to HED meteorites (Trinquier et al., 2007, 2009). When ordinary chondrites are taken as the HED starting material, the slope in a Δ^{199}Hg versus Δ^{201}Hg diagram is 1.82 ± 0.29 (Fig. 3A). Similar results, within error, are obtained when carbonaceous chondrites (1.79 ± 0.15) or enstatite chondrites (1.67 ± 0.14) are used as the starting materials (Fig. 3B, 3C). In Fig. 3 we include both the data obtained here (Dhofar 007) and the one analysis previously published (Millbillillie, Meier et al., 2016), the two other data points have only been reported in abstracts and are not available. These correlations are what would be expected for an isotopic fractionation under an equilibrium control by the NFSE (assuming the slope estimated from low temperature experiments and calculations holds at magmatic temperatures). The Hg isotopic composition of the eucrites, therefore suggests Hg loss by evaporation (heavy stable isotope enrichment) under an equilibrium condition, as previously suggested for Cr (Zhu et al., 2019). Here we show that Hg isotopes are critical for testing the condition of evaporation as demonstrated by the relationship between two odd-MIF. To fully demonstrate this effect, additional eucrite meteorites should be analyzed in the future. With the addition of Hg isotopic data on lunar samples, this methodology will be valuable in the future to test lunar volatile loss which is presently highly debated (Sharp et al., 2010; Paniello et al., 2012b; Boyce et al., 2015; Kato et al., 2015; Pringle and Moynier, 2017; Wang and Jacobsen, 2016; Wang et al., 2019; Day et al., 2020)

4.3. A terrestrial Hg isotope signature dominantly controlled by late accretion?

The eight terrestrial igneous rocks analyzed here (δ^{202}Hg between −4.95 and −2.42) have isotopic compositions mostly consistent with the data reported in Geng et al. (2018) (e.g. two basalts, BHVO-2 and BCR-2 have a δ^{202}Hg of −2.44 and −2.08 respectively, one andesite GSR-2 has a δ^{202}Hg of −1.47) but clearly heavier than what had been reported in Smith et al. (2009). Smith et al. (2009) reported data for several igneous rocks from the California coast ranges (USA), including basalts, dacites and rhyolites. These samples have δ^{202}Hg between −1.2 and −0.46, therefore falling within the range of sedimentary rock compositions. On the other hand, all these samples are highly enriched in Hg compared to the igneous rocks presented here (up to 300 ppb vs a few ppb in our basalts) suggesting Hg contamination from sediment was likely during the significant (15-40%) crustal assimilation sustained by these rocks (Hammersley and Depaolo, 2006). To a first order, many igneous rock types that suffered no (or, at least, more limited) crustal assimilation should be better samples to characterize the composition of the terrestrial silicate composition as these rocks are formed by melting of mantle source rocks. The question is whether the values obtained from igneous rocks represent the composition of Earth's mantle given the high volatility of Hg leading to potential isotopic fractionation during degassing (e.g. Zambardi et al., 2009; Sherman et al., 2009), and potential isotopic fractionation during magmatic differentiation as observed for other metals (e.g. Deng et al., 2018; Inglis et al., 2019; Schuessler et al., 2009). Volatilization is known to strongly fractionate moderately volatile elements and their isotopes such as Zn or Cd (e.g. Moynier et al., 2017; Wombacher et al., 2008). During degassing it would be expected that the gas would be enriched in the lighter isotopes, leaving an isotopically heavy residue behind. For example, this is what Zambardi et al. (2009) observed for Hg between fumarolic gas and condensed particles of Vulcano Island, with an isotopic fractionation factor for the ^{202}Hg/^{198}Hg ratio between solid and gas that was greater than one. In that case study, the value ob-

tained for degassed igneous rocks would be enriched in the heavier Hg isotopes compared to their source rocks. However, because the rocks analyzed lack a genetic relationship, and because the rocks are derived from sources that possibly had different Hg contents, different degrees of melting, or different temperature, it is not possible to calculate the Hg isotopic composition of the mantle source based on these data.

Magmatic processes, such as partial melting or fractional crystallization, are also known to produce isotopic fractionation which could also lead to the isotopic variability (e.g. Deng et al., 2018; Schuessler et al., 2009). This effect can contribute to the isotopic variability observed among the igneous rocks. However, given what is observed for much lighter elements (the effect is <1 permil for even the most extreme cases, e.g. Deng et al., 2018; Schuessler et al., 2009), and that the traditional isotopic fractionation is proportional to the relative mass difference, we would not expect fractional crystallization to generate the large (~2 permil) δ^{202}Hg variability observed in the terrestrial samples reported here. It is possible that, during igneous petrogenesis, the isotopic fractionation would be controlled by the nuclear field shift effect (e.g. Bigeleisen, 1996), but elements of similar mass such as Tl, do not show resolvable isotopic fractionation within 0.1 permil (Nielsen et al., 2017). Furthermore, in terms of MIF, while none of the igneous rocks analyzed here show strong isotopic effects, there is a weak negative trend between Δ^{199}Hg and δ^{202}Hg (Fig. 5), with the largest $\Delta^{199}\text{Hg} = 0.06 \pm 0.03$ (2sd) for the isotopically lightest sample ($\delta^{202}\text{Hg} = -4.95 \pm 0.08$) (Table 2). The range of MIF is consistent with what has been observed for volcanic gas from Vulcano, Italy (Zambardi et al., 2009), and in samples from hot springs from the Yellowstone Plateau volcanic field and vent chimney samples from the Guaymas Basin sea-floor rift, USA (Sherman et al., 2009) where Δ^{199}Hg up to 0.22 was observed. The limited correlation between the MDF and MIF is not surprising given that all samples are unrelated rocks (and therefore are not linked by a common process, e.g., degassing, fractional crystallization). However, it should be noted that there is generally a weak negative trend (Fig. 5, slope of -0.023 ± 0.016, 1σ, when all samples are included), consistent with kinetic evaporation experiments made by Estrade et al. (2009) (Slope of -0.014 ± 0.001). As mentioned previously, the Estrade et al. (2009) experiments were conducted in conditions (pure Hg, low temperature, vacuum) irrelevant to magmatic degassing, and the magnitude of the isotopic fractionation and the slope in a Δ^{199}Hg versus δ^{202}Hg plot may be affected by the experimental conditions. While we acknowledge this caveat and the uncertainty in the slope of the trend formed by terrestrial igneous data in Δ^{199}Hg versus δ^{202}Hg space, we suggest that the ~2 permil isotopic variability among igneous rocks is mainly controlled by degassing, and we thus infer that their source rocks must have an isotopic composition even lighter than the igneous samples. Alternatively, it is possible that some of the isotopically light Hg represents contamination by isotopically light vapor. In this unlikely event, all eight igneous rocks analyzed so far would have been contaminated by isotopically light vapor. More data will be required to fully test the origin of the isotopically light igneous rocks.

These results point to a terrestrial igneous δ^{202}Hg composition that is significantly lighter than previously suggested and that the mantle exhibits limited MIF of Hg. Until a more quantitative assessment can be made, based on a larger variety of igneous rocks and on mantle peridotites, we suggest the Earth's mantle has a $\delta^{202}\text{Hg} < -2.35$, which is more than 1 permil lighter than the previous assessment based on sedimentary rocks. The heavy isotopic enrichment of sedimentary rocks compared to the igneous rocks suggests further isotopic fractionation by geological processes such as Hg degassing, weathering, sorption/desorption and an isotopically light reservoir must complement the isotopically heavy sediments.

Thus, contrary to the earlier mantle δ^{202}Hg estimate, terrestrial igneous rocks falls within the range defined by chondrites in MDF (Fig. 4). The Hg abundance and isotopic composition of Hg recorded in terrestrial igneous rocks may have been affected by any one, or a combination of, the following processes: 1) core formation; 2) volatilization during accretion, and 3) late accretion.

The concentration of Hg in the bulk Earth is not well known, as it is presently not possible to accurately determine the fraction of Hg partitioned into the core as no metal/silicate/sulphide experimental data presently exists. Based on concentration measurements in peridotites and crustal rocks, Canil et al. (2015) suggested a concentration of 0.4 to 0.6 ppb of Hg in Earth's upper mantle. On the other hand, estimates based on the continental crust composition and considering elemental ratios (e.g. Se/Hg ratio) lead to higher values, for example Salters and Stracke (2004) suggest 10 ppb and Palme and O'Neill (2003) 6 ppb. The Hg content of the Earth's mantle is therefore unclear. In any case, Hg is highly depleted in Earth's mantle compared to CI chondrites, possibly in the same range as for Se, Te and S (Canil et al., 2015). Another strong limitation of this approach is that the concentration of Hg in CI chondrites is highly variable and it is therefore difficult to constrain the composition for the whole CI parent body. Furthermore, Hg is one of the elements for which we have no accurate solar composition (e.g. Grevesse et al., 2015), which limits the estimate of its cosmic abundance. To illustrate the large uncertainty on the Hg content of CI chondrites, Meier et al. (2016), Wiederhold and Schönbächler (2015) and our study point to a much higher Hg content (>13,000 ppb) in CI than that proposed by Canil et al. (2015) or Palme et al. (2014) as the CI reference value (350 ppb). The Hg concentration reported in Palme et al. (2014) is actually not based on measurements in CI chondrites, but is reported from Anders and Grevesse (1989) which is estimated from nucleosynthetic modeling. Using a similar approach Lauretta et al. (1999) estimated the Hg abundance of the solar system to be 258 ppb. However, if we consider 13,000 ppb as the Hg concentration in CI, Hg would be ~40 times more depleted in the mantle compared to CI chondrites as suggested in Canil et al. (2015).

The large difference in the Hg abundance in CI chondrites between modeling and measurements may be reconciled if we consider that fluid alteration or thermal metamorphism (Springmann et al., 2019) of Orgueil enriched its surface in Hg compared to the whole parent body and that collected samples do not represent the whole CI parent body. Whatever estimate is considered, Hg is highly depleted in Earth compared to where it should be if it was solely controlled by volatilization processes, as suggested by Canil et al. (2015). The extreme depletion of Hg in mantle-derived terrestrial igneous rocks points toward a siderophilic behavior of Hg at high pressure and major partitioning of Hg into the Earth's core and/or extreme degassing loss during its accretion.

The extreme uncertainties in the Hg abundance of both Earth's mantle and CI chondrites make it difficult to meaningfully quantify core segregation and late accretion modification of terrestrial Hg budgets. Instead, the isotopic composition of Hg can be used as a tool to quantify the relative proportion of the different processes. Since there are presently no experimental data of the high-pressure high-temperature isotopic behavior of Hg, it is not possible to estimate isotopic fractionation during partitioning of Hg in Earth's core. Our present estimate for terrestrial δ^{202}Hg falls within the chondritic range, and makes late accretion of carbonaceous chondrite-like material possible for explaining the terrestrial Hg content. Given the usual estimate of the amount of late accreting material to Earth (~0.5%, Day et al., 2016) necessary to explain the HSE budget of the mantle, and taking a minimum Hg content of ~258 ppb (Lauretta et al., 1999), we obtain a Hg content

for the Earth's mantle of ~2ppb, which falls between estimates by Canil et al. (2015) (~0.5 ppb) and Salters and Stracke (2004) (10 ppb), therefore making late accretion of Hg a possible source for the mantle composition. This would be in agreement with prior suggestions for the origin of volatile elements in the Earth: Marty (2012) for N, C and noble gases, Meier et al. (2016) for Hg, Wang and Becker (2013) for S, Se and Te and Varas-Reus et al. (2019) for Se. Given the large range of estimates for both chondrites and Earth's mantle Hg, this mass-balance does not exclude the possibility that a fraction of mantle Hg originated from metal/silicate differentiation.

Mass-independent fractionation of Hg isotopes could also be used to provide additional constraints on the origin of mantle Hg and decipher between the chondrite groups that may have participated in the late accretion of Hg. While within one chondritic group (and even within a single sample, Table 1) a range of MIF is found, the limited terrestrial MIF suggests that terrestrial Hg is either closer to OC or CO chondrites. On the other hand, non-CO CC and EH chondrites exhibit generally larger MIF than that observed in terrestrial igneous rocks. If these meteorite groups were to dominate the terrestrial late accretion budget (as suggested by Se isotopic compositions Varas-Reus et al., 2019) and noble gases (Bekaert et al., 2020), the Earth's Hg budget would have to be controlled by core formation. Refining of the Earth's Hg MDF isotopic composition and future metal/silicate experiments will be necessary to test these scenarios (Fig. 4).

5. Conclusions

While highly variable in Hg isotopic composition ($-4.95 < \delta^{202}\mathrm{Hg} < -2.35$), terrestrial igneous rocks are isotopically lighter than sedimentary rocks that were previously used as representative of mantle composition. We propose that the isotopic variability is due to magmatic degassing and that the mantle composition must be at least lower than -2.35. Our chondrite data are consistent with previous work for carbonaceous chondrites (positive odd-MIF), ordinary chondrites (no odd-MIF) and we provide the first values for enstatite chondrites from which some exhibit positive odd-MIF similar to carbonaceous chondrites. Terrestrial igneous rocks fall within the general range of chondritic isotopic composition. We suggest that Hg could have been delivered by late accretion as previously suggested for other volatile chalcophile elements, S, Se and Te. Considering the MIF, CO chondrites or ordinary chondrites are the most likely candidates, if the Hg content of the present Earth is dominated by late accretion. However, it cannot be excluded that all or a fraction of the mantle Hg budget was modified further by core formation or degassing during a giant impact phase. Future high-pressure, high-temperature experiments are thus necessary to test these scenarios. Finally, the eucrite meteorite data is consistent with previous data, being isotopically heavier than chondrites and having negative odd-MIF. We show that the $\Delta^{199}\mathrm{Hg}$ versus $\Delta^{201}\mathrm{Hg}$ relation points toward an equilibrium nuclear field shift effect in eucrite meteorites, suggesting that the asteroid Vesta (the most likely parent body for the eucrite meteorites) lost its volatile during degassing of a magma ocean phase.

CRediT authorship contribution statement

FM and JBC: designed the study. **JBC, KC, HC:** performed the measurements. **FM, JBC, JMDD, MGJ, ZW:** discussed and interpreted the data. **FM:** wrote the manuscript with the help of JBC, JMDD, ZW and MGJ.

Declaration of competing interest

The authors declare that they have no known competing financial interests or personal relationships that could have appeared to influence the work reported in this paper.

Acknowledgements

We thank Mathias Meier and an anonymous reviewer for very insightful comments that greatly improved the paper. Raj Dasgupta is thanked for efficient editorial handling. FM thanks Guillaume Avice for fruitful discussions. This study was supported by the National Natural Science Foundation of China (41625012, 41961144028, U1612442, 41830647) to JBC and by the China National Space Administration (No. D020205) to ZW. FM thanks Yongsheng Liu for making the visit at CUG Wuhan possible. MGJ thanks IPGP for providing a stimulating academic home during sabbatical, and acknowledges partial support from NSF EAR-1900652.

Appendix A. Supplementary material

Supplementary material related to this article can be found online at https://doi.org/10.1016/j.epsl.2020.116544.

References

Anders, E., Grevesse, N., 1989. Abundances of the elements: meteoritic and solar. Geochim. Cosmochim. Acta 53, 197–214.
Bekaert, D., Broadley, M., Marty, B., 2020. The origin and fate of volatile elements on Earth revisited in light of noble gas data obtained from comet 67P/Churyumov-Gerasimenko. Sci. Rep. 10, 5796.
Bergquist, B.A., Blum, J.D., 2007. Mass-dependent and-independent fractionation of Hg isotopes by photoreduction in aquatic systems. Science 318, 417–420.
Bigeleisen, J., 1996. Nuclear size and shape effects in chemical reactions. Isotope chemistry of the heavy elements. J. Am. Chem. Soc. 118, 3676–3680.
Blum, J., Popp, B., Drazen, J., Choy, C., Johnson, M., 2013. Evidence for methylmercury production below the mixed layer in the central North Pacific Ocean. Nat. Geosci. 6, 879–884.
Blum, J., Sherman, L., Johnson, M.W., 2014. Mercury isotopes in Earth and environmental sciences. Annu. Rev. Earth Planet. Sci. 42, 249–269.
Blum, J., Johnson, M.W., 2017. Recent developments in mercury stable isotopes analysis. In: Teng, F.-Z., Watkins, J., Dauphas, N. (Eds.), Non-Traditional Stable Isotopes. Mineralogical Society of America, pp. 733–757.
Boyce, J., Treiman, A., Guan, Y., Ma, C., Eiler, J., Gross, J., Greenwood, J., Stolper, E., 2015. The chlorine isotope fingerprint of the lunar magma ocean. Sci. Adv. 8, e1500380.
Braukmüller, N., Wombacher, F., Funk, C., Münker, C., 2019. Earth's volatile element depletion pattern inherited from a carbonaceous chondrite-like source. Nat. Geosci. 12, 564–568.
Canil, D., Crockford, P., Rossin, R., Teimer, K., 2015. Mercury in some arc crustal rocks and mantle peridotites and relevance to the moderately volatile element budget of the Earth. Chem. Geol. 396, 134–142.
Caillet Komorowski, C., El Goresy, A., Miyahara, M., Boudouma, O., Ma, C., 2012. Discovery of Hg-Cu-bearing metal-sulfide assemblages in a primitive H-3 chondrite: towards a new insight in early solar system processes. Earth Planet. Sci. Lett. 349–350, 261–271.
Chen, J., Hintelmann, H., Dimock, B., 2010. Chromatographic pre-concentration of Hg from dilute aqueous solutions for isotopic measurement by MC-ICP-MS. J. Anal. At. Spectrom. 25, 1402–1409.
Chen, J., Hintelmann, H., Feng, X., Dimock, B., 2012. Unusual fractionation of both odd and even mercury isotopes in precipitation from Peterborough, ON, Canada. Geochim. Cosmochim. Acta 90, 33–46.
Creech, J., Moynier, F., 2019. Tin and zinc stable isotope characterisation of chondrites and implications for early Solar System evolution. Chem. Geol. 511, 81–90.
Dale, C., Burton, K., Greenwood, R., Gannnoun, A., Wade, J., Wood, B., Pearson, G., 2012. Late accretion on the earliest planetesimals revealed by the highly siderophile elements. Science 336, 72–75.
Day, J.M.D., Moynier, F., 2014. Evaporative fractionation of volatile stable isotopes and their bearing on the origin of the Moon. Philos. Trans. A 372, 20130259.
Day, J.M.D., Pearson, D.G., Taylor, L.A., 2007. Highly siderophile element constraints on accretion and differentiation of the Earth-Moon system. Science 315, 217–219.
Day, J.M.D., Walker, R.J., Brandon, A.D., 2016. Highly siderophile elements in Earth, the Moon, Mars and asteroids. In: Harvey, J., Day, J.M.D. (Eds.), Rev. Min. Geo., vol. 81. Mineralogical Society of America, pp. 161–238.

Day, J.M.D., Van Kooten, E., Hofmann, B., Moynier, F., 2020. Mare basalt meteorites, magnesian-suite rocks and KREEP reveal loss of zinc during and after lunar formation. Earth Planet. Sci. Lett. 531, 115998.
Deng, Z., Chaussidon, M., Savage, P., Robert, F., Pik, R., Moynier, F., 2018. Titanium isotopes as a tracer for the plume or island arc affinity of felsic rocks. Proc. Natl. Acad. Sci. USA 116, 1132–1135.
Estrade, N., Carignan, J., Sonke, J.E., Donard, O., 2009. Mercury isotope fractionation during liquid-vapor evaporation experiments. Geochim. Cosmochim. Acta 73, 2693–2711.
Estrade, N., Carignan, J., Donard, O., 2010. Isotope tracing of atmospheric mercury sources in an urban area of northeastern France. Environ. Sci. Technol. 44, 6062–6067.
Fischer-Gödde, M., Elfers, B.M., Münker, C., Szilas, K., Maier, W., Messling, N., Morishita, T., Van Kranendonk, M., Smithies, H., 2020. Ruthenium isotope vestige of Earth's pre-late-veneer mantle preserved in Archaean rocks. Nature 579, 240–244.
Foucher, D., Hintelmann, H., 2006. High-precision measurement of mercury isotope ratios in sediments using cold-vapor generation multi-collector inductively coupled plasma mass spectrometry. Anal. Bioanal. Chem. 384, 1470–1478.
Geng, H., Yin, R., Li, X., 2018. An optimized protocol for high precision measurement of Hg isotopic compositions in samples with low concentrations of Hg using MC-ICP-MS. J. Anal. At. Spectrom. 33, 1932–1940. https://doi.org/10.1039/C8JA00255J.
Ghosh, S., Schauble, E., Couloume, G., Blum, J., Bergquist, B.A., 2013. Estimation of nuclear volume dependent fractionation of mercury isotopes in equilibrium liquid–vapor evaporation experiments. Chem. Geol. 336, 5–12.
Grevesse, N., Scott, P., Asplund, M., Sauval, J., 2015. The elemental composition of the Sun III. The heavy elements Cu to Th. Astron. Astrophys. 573, A27.
Hammersley, L., Depaolo, D., 2006. Isotopic and geophysical constraints on the structure and evolution of the Clear Lake volcanic system. J. Volcanol. Geotherm. Res. 153, 331–356.
Huang, Q., Chen, J., Huang, W., Reinfelder, J.R., Fu, P., Yuan, S., Wang, Z., Yuan, W., Cai, H., Ren, H., 2019. Diel variation in mercury stable isotope ratios records photo-reduction of PM 2.5-bound mercury. Atmos. Chem. Phys. 10, 315–325.
Huang, Q., Liu, Y., Chen, J., Feng, X., Huang, W., Yuan, S., Cai, H., Fu, X., 2015. An improved dual-stage protocol to pre-concentrate mercury from airborne particles for precise isotopic measurement. J. Anal. At. Spectrom. 30, 957–966.
Inglis, E., Moynier, F., Creech, J., Deng, Z., Day, J.M.D., Teng, F.-Z., Bizzarro, M.M.J., Savage, P., 2019. Isotopic fractionation of zirconium during magmatic differentiation and the stable isotope composition of the silicate Earth. Geochim. Cosmochim. Acta 250, 311–323.
Javoy, M., Kaminski, E., Guyot, F., Andrault, D., Sanloup, C., Moreira, M., Labrosse, S., Jambon, A., Agrinier, P., Davaille, A., Jaupart, C., 2010. The chemical composition of the Earth: enstatite chondrite models. Earth Planet. Sci. Lett. 293, 259–268.
Kato, C., Moynier, F., Valdes, M.C., Dhaliwal, J.K., Day, J.M.D., 2015. Extensive volatile loss during formation and differentiation of the Moon. Nat. Commun. 6, 7617.
Lauretta, D., Devouard, B., Buseck, P., 1999. The cosmochemical behavior of mercury. Earth Planet. Sci. Lett. 171, 37–47.
Lauretta, D., Klaue, B., Blum, J., Buseck, P., 2001. Mercury abundances and isotopic compositions in the Murchison (CM) and Allende (CV) carbonaceous chondrites. Geochim. Cosmochim. Acta 65, 2807–2818.
Luck, J.M., Othman, D.B., Albarede, F., 2005. Zn and Cu isotopic variations in chondrites and iron meteorites: early solar nebula reservoirs and parent-body processes. Geochim. Cosmochim. Acta 69, 5351–5363.
Marty, B., 2012. The origins and concentrations of water, carbon, nitrogen and noble gases on Earth. Earth Planet. Sci. Lett. 314, 56–66.
Meier, M., Cloquet, C., Marty, B., 2016. Mercury (Hg) in meteorites: variations in abundance, thermal release profile, mass-dependent and mass-independent isotopic fractionation. Geochim. Cosmochim. Acta 182, 55–72.
Moynier, F., Vance, D., Fujii, T., Savage, P., 2017. The isotope geochemistry of copper and zinc. In: Teng, F.-Z., Watkins, J., Dauphas, N. (Eds.), Non-Traditional Stable Isotopes. In: Rev. Min. Geo., vol. 82. Mineralogical Society of America, pp. 543–600.
Nielsen, S.G., Rehkaemper, M., Prytulak, J., 2017. Investigation and application of thallium isotope fractionation. In: Teng, F.-Z., Watkins, J., Dauphas, N. (Eds.), Non-Traditional Stable Isotopes. In: Rev. Min. Geo., vol. 82. Mineralogical Society of America, pp. 759–798.
O'Neill, H.S.C., Palme, H., 2008. Collisional erosion and the non-chondritic composition of the terrestrial planets. Phil0s. Trans. R. Soc. A 366, 4205–4238.
O'Nions, R., Hamilton, P., Evensen, N., 1977. Variations in $^{143}Nd/^{144}Nd$ and $^{87}Sr/^{86}Sr$ ratios in oceanic basalts. Earth Planet. Sci. Lett. 34, 13–22.
Palme, H., O'Neill, H., 2003. Cosmochemical estimates of Mantle composition. In: Holland, H.D., Turekian, K.K. (Eds.), Treatise on Geochemistry, pp. 1–38.
Palme, H., Lodders, K., Jones, A., 2014. Solar system abundances of the elements. In: Holland, H.D., Turekian, K.K. (Eds.), Treatise in Geochemistry. Elsevier, Amsterdam, pp. 41–61.
Paniello, R.C., Moynier, F., Beck, P., Barrat, J.A., Podosek, F.A., Pichat, S., 2012a. Zinc isotopes in HEDs: clues to the formation of 4-Vesta, and the unique composition of Pecora Escarpment 82502. Geochim. Cosmochim. Acta 86, 76–87.
Paniello, R.C., Day, J.M.D., Moynier, F., 2012b. Zinc isotopic evidence for the origin of the Moon. Nature 490, 376–379.
Poitrasson, F., Halliday, A.N., Lee, D.-C., Levasseur, S., Teutsch, N., 2004. Iron isotope differences between Earth, Moon, Mars and Vesta as possible records of contrasted accretion mechanisms. Earth Planet. Sci. Lett. 223, 253–266.
Pringle, E., Moynier, F., 2017. Rubidium isotopic composition of the Earth, meteorites, and the Moon: evidence for the origin of volatile loss during planetary accretion. Earth Planet. Sci. Lett. 473, 62–70.
Pringle, E., Moynier, F., Beck, P., Paniello, R., Hezel, D.C., 2017. The origin of volatile element depletion in early solar system material: clues from Zn isotopes in chondrules. Earth Planet. Sci. Lett. 468, 62–71.
Salters, V.J.M., Stracke, A., 2004. Composition of the depleted mantle. Geochem. Geophys. Geosyst. 5. https://doi.org/10.1029/2003GC000597.
Savage, P., Moynier, F., Chen, H., Shofner, G., Siebert, J., Badro, J., Puchtel, I.S., 2015. Copper isotope evidence for large-scale sulphide fractionation during Earth's differentiation. Geochem. Perspect. Lett. 1, 53–64.
Schuessler, J., Schoenberg, R., Sigmarsson, O., 2009. Iron and lithium isotope systematics of the Hekla volcano, Iceland — evidence for Fe isotope fractionation during magma differentiation. Chem. Geol. 258, 78–91.
Sharp, Z., Shearer, C., McKeegan, K., Barnes, J., Wand, Y., 2010. The chlorine isotope composition of the moon and implications for an anhydrous mantle. Science 329, 1050–1053.
Sherman, L., Blum, J., Nordstrom, D., 2009. Mercury isotopic composition of hydrothermal systems in the Yellowstone Plateau volcanic field and Guaymas Basin sea-floor rift. Earth Planet. Sci. Lett. 279, 86–96.
Sherman, L., Blum, J., Johnson, K., Keeler, G., Barres, J., Douglas, T., 2010. Mass-independent fractionation of mercury isotopes in Arctic snow driven by sunlight. Nat. Geosci. 3, 173–177.
Siebert, J., Sossi, P.A., Blanchard, I., Mahan, B., Badro, J., Moynier, F., 2018. Chondritic Mn/Na ratio and limited post-nebular volatile loss to the Earth. Earth Planet. Sci. Lett. 485, 130–139.
Smith, C.N., Kesler, S., Blum, J., Rytuba, J., 2009. Isotope geochemistry of mercury in source rocks, mineral deposits and spring deposits of the California Coast Ranges, USA. Earth Planet. Sci. Lett. 269, 399–407.
Sonke, J., Schafer, J., Chmeleff, J., Audry, S., Blanc, G., Dupre, B., 2010. Sedimentary mercury stable isotope records of atmospheric and riverine pollution from two major European heavy metal refineries. Chem. Geol. 279, 90–100.
Springmann, A., Lauretta, D., Klaue, B., Goreva, Y., Blum, J., Andronikov, A., Steckloff, J., 2019. Thermal alteration of labile elements in carbonaceous chondrites. Icarus 324, 104–119.
Steenstra, E., Lin, Y., Dankers, D., Rai, N., Berndt, J., Matveev, S., van Westrenen, W., 2017. The lunar core can be a major reservoir for volatile elements S, Se, Te and Sb. Sci. Rep. 7, 14552.
Tian, Z., Chen, H., Fegley Jr, B., Lodders, K., Barrat, J.A., Day, J.M.D., Wang, K., 2019. Potassium isotopic compositions of howardite-eucrite-diogenite meteorites. Geochim. Cosmochim. Acta 266, 611–632.
Trinquier, A., Birck, J.-L., Allègre, C.J., 2007. Widespread ^{54}Cr heterogeneity in the inner Solar system. Astrophys. J. 655, 1179–1185.
Trinquier, A., Elliott, T., Ulfbeck, D., Coath, C., Krot, A.N., Bizzarro, M., 2009. Origin of nucleosynthetic isotope heterogeneity in the Solar Protoplanetary Disk. Science 324, 374–376.
Varas-Reus, M.I., Konig, S., Yierpan, A., Lorand, J.P., Schoenberg, R., 2019. Selenium isotopes as tracers of a late volatile contribution to Earth from the outer Solar System. Nat. Geosci. 12, 779–782.
Vollstaedt, H., Mezger, K., Leya, I., 2016. The isotope composition of selenium in chondrites constrains the depletion mechanism of volatile elements in solar system materials. Earth Planet. Sci. Lett. 450, 372–380.
Wang, K., Jacobsen, S.B., 2016. Potassium isotopic evidence for a high-energy giant impact origin of the Moon. Nature 538, 487–490.
Wang, X., Fitoussi, C., Bourdon, B., Fegley, B., Charnoz, S., 2019. Tin isotopes indicative of liquid–vapour equilibration and separation in the Moon-forming disk. Nat. Geosci. 12, 707–711.
Wang, Z.Z., Becker, H., 2013. Ratios of S, Se and Te in the silicate Earth require a volatile-rich late veneer. Nature 499, 328–331.
Wiederhold, J.G., Schönbächler, M., 2015. Mercury concentrations and Hg isotope compositions of chondrites and eucrites. In: LPI (Ed.), Lunar Planet. Sci. Conf. Houston. Abstract 1841.
Wombacher, F., Rehkämper, M., Mezger, K., Bischoff, A., Münker, C., 2008. Cadmium stable isotope cosmochemistry. Geochim. Cosmochim. Acta 72, 646–667.
Yuan, S., Chen, J., Cai, H., Yuan, W., Wang, Z., Huang, Q., Liu, Y., Wu, X., 2018. Sequential samples reveal significant variation of mercury isotope ratios during single rainfall events. Sci. Total Environ. 624, 133–144.
Zambardi, T., Sonke, J., Toutain, J.-P., Sortnob, F., Shinoharac, H., 2009. Mercury emissions and stable isotopic compositions at Vulcano Island (Italy). Earth Planet. Sci. Lett. 277, 236–243.
Zhang, Y., Chen, J., Zheng, W., Sun, R., Yuan, S., Cai, H., Au Yang, D., Yuan, W., Meng, M., Wang, Z., Liu, Y., Liu, J., 2020. Mercury isotope compositions in large anthropogenically impacted Pearl River, South China. Ecotoxicol. Environ. Saf. 191, 110229.
Zhu, K., Sossi, P., Siebert, J., Moynier, F., 2019. Tracking the volatile and magmatic history of Vesta from chromium stable isotope variations in eucrite and diogenite meteorites. Geochim. Cosmochim. Acta 266, 598–610.